





Solid-Electrolyte Interphase Hot Paper

How to cite: *Angew. Chem. Int. Ed.* **2025**, *64*, e202505832 doi.org/10.1002/anie.202505832

Mediating Solid Electrolyte Interphase Formation Kinetics on SiO_x Anodes Using Proton Acceptors

Haoliang Wang⁺, Hao Zhang⁺, Lu Wang, Zhibo Song, Wenguang Zhao, Zhaohuang Zhan, Jianjun Fang, Yuxiang Huang, Zu-Wei Yin, Feng Pan,* and Luyi Yang*

Abstract: Silicon (Si)-based anodes offer high energy density but suffer from significant volume variations, leading to an unstable solid electrolyte interphase (SEI). To enhance SEI stability, numerous electrolyte additives have been designed to decompose on the anode and form desirable SEI components (e.g., LiF). However, their electrochemical reduction kinetics on the anode surface competes with other electrolyte components, leading to suboptimal interfacial decomposition efficiency and a less stable SEI structure. Here, inspired by bioremediation strategies in petroleum pollution treatment, we introduce a proton acceptor that reacts with fluoroethylene carbonate (FEC), a commercially established additive, to generate an intermediate. Such an intermediate lowers the reduction kinetic barrier, accelerating the formation of LiF and enriching it in the inner layer of the SEI. Compared to the randomly distributed LiF structure, the resulting SEI exhibits better mechanical stability and lithium-ion conduction, effectively accommodating volume changes and mitigating stress concentration caused by local overlithiation. As a result, the electrochemical performance surpasses that of previously reported works. This intermediate-based strategy significantly improves the utilization efficiency of commercial additives, offering a practical direction for future electrolyte design.

Introduction

Exhibiting high specific capacities, low operating voltages, and low costs, Si-based anodes have attracted significant interest from researchers as a leading candidate for high-energy-density lithium-ion batteries. Nonetheless, the high capacity of Si-based anodes is accompanied by high volumetric variation rates, which could lead to a series of issues, including particle pulverization, electrode disintegration, and the repeated fracturing and regeneration of the SEI. Previously, it has been revealed that excessive SEI growth on SiO_x (0 < x < 2) anodes could disrupt charge transfer networks, causing capacity fading. Recent years have witnessed significant progress in designing a

durable and chemically stable SEI on Si-based anodes, including structural design, [11] electrolyte engineering, [12] and binder optimization. [13] Especially, the decomposition of the electrolyte on the anode surface plays a crucial role in determining the composition and structure of the SEI.

Compared to the organic SEI components derived from carbonate solvents, inorganic SEI components represented by LiF are considered more ideal due to their chemical and mechanical stability.[14-17] Therefore, fluorine (F)-containing electrolyte additives with suitable lowest unoccupied molecular orbital (LUMO) energy levels have been the subject of extensive research due to their ability to construct a stable, LiF-rich SEI.[18-20] As a commercialized electrolyte additive, FEC has been extensively used to enhance the performance of Si-based anodes.[21,22] Through electrochemical reduction within a voltage window of 1.0 to 1.4 V versus Li/Li+, FEC helps to form an SEI consisting of polymerized vinylene carbonate, lithium carbonate (Li₂CO₃), and LiF.^[23,24] This composition not only promotes rapid lithium-ion conduction at the interphase but also effectively adapts to the volumetric swings of Si-based anodes. [25,26] Despite being regarded as one of the most commercially successful and widely used filmforming additives, the decomposition process of FEC remains uncontrollable. The high energy barrier associated with this electrochemical reduction often results in incomplete FEC decomposition during the initial cycles, leading to the formed LiF having not only a low compositional proportion in the SEI, but more importantly, its distribution is random and uncontrollable. Due to the lack of consistency, the resulting SEI will suffer from uneven lithium-ion transport and surface stress, adversely affecting the cycling and rate performance of the anode.^[27,28] In order to regulate the reduction process

Z. Song

Hefei National Research Center for Physical Sciences at the Microscale, CAS Key Laboratory of Materials for Energy Conversion, Department of Materials Science and Engineering, University of Science and Technology of China, Anhui 230026, China

Z.-W. Yin

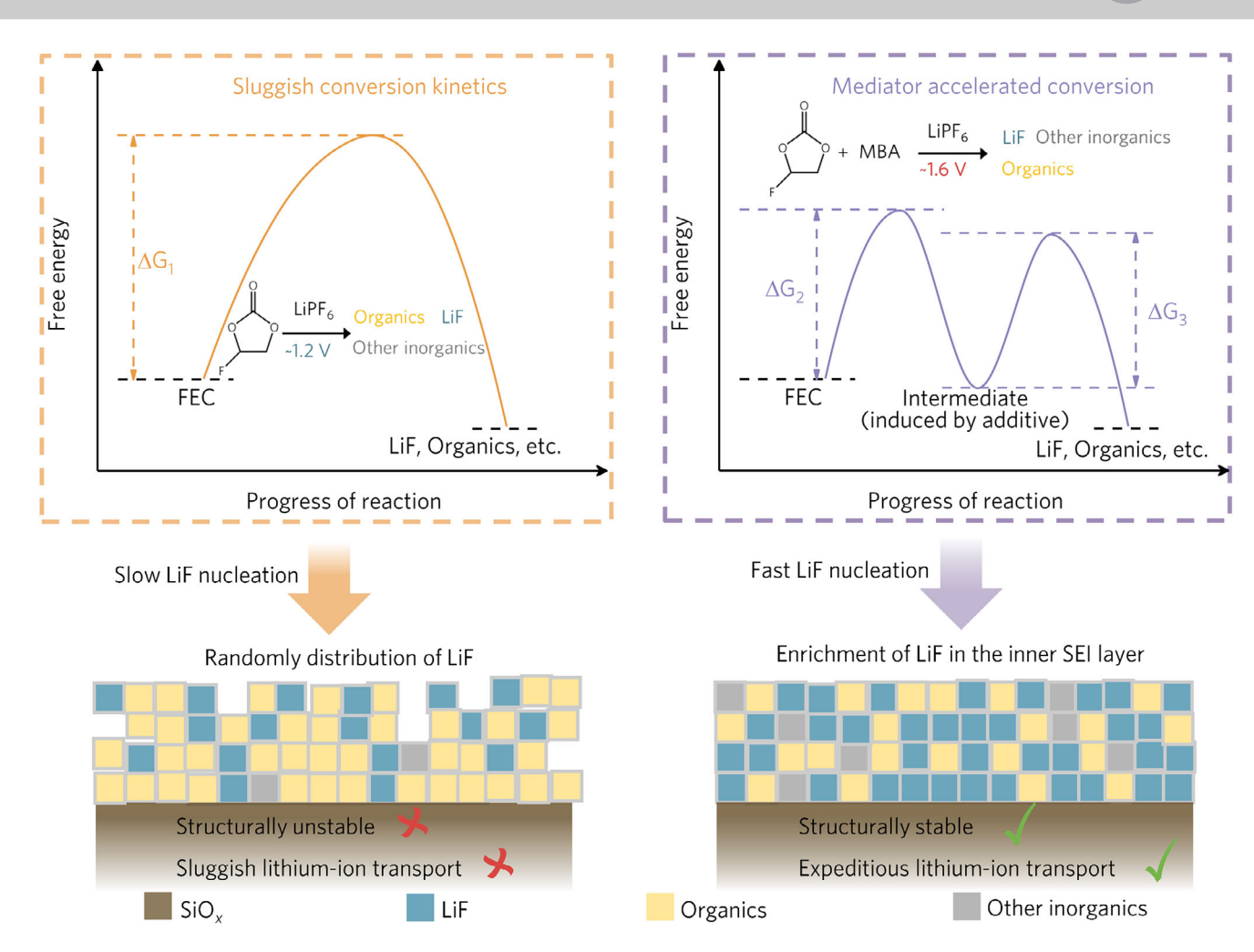
College of Energy, Xiamen University, Xiamen 361005, China

- [+] Both authors contributed equally to this work.
- Additional supporting information can be found online in the Supporting Information section

^[*] H. Wang⁺, H. Zhang⁺, L. Wang, W. Zhao, Z. Zhan, J. Fang, Y. Huang, F. Pan, L. Yang School of Advanced Materials, Peking University Shenzhen Graduate School, Shenzhen 518055, China E-mail: panfeng@pkusz.edu.cn yangly@pkusz.edu.cn

15213773, 2025, 33, Downloaded from https://onlinelibrary.wiley.com/doi/10.1002/anie.202505832 by University Town Of Shenzhen, Wiley Online Library on [17/11/2025]. See the Terms

ns) on Wiley Online Library for rules of use; OA articles are governed by the applicable Creative Commons



Scheme 1. Design concept and mechanism of MBA-induced rapid LiF nucleation for constructing an SEI with a LiF-rich inner layer.

of FEC, MoSe₂ coating layer has been applied on the Si anode.^[29] This coating exhibits a high adsorption affinity for FEC molecules, facilitating the decomposition reaction of FEC and leading to the formation of an SEI enriched with polymerized vinylene carbonate and LiF. However, due to the limited feasibility of such solutions in practical applications, a new approach that is more compatible with the current battery manufacturing process needs to be proposed.

Inspired by bioremediation techniques that use microbial metabolism to decompose complex petroleum hydrocarbons (e.g., alkanes and aromatic hydrocarbons) into smaller molecules (e.g., alcohols, acids, and ketones), [30,31] a novel coadditive, bis(2-methoxyethyl)amine (MBA) is introduced to accelerate the conversion of commercial electrolyte additive FEC into the target LiF product. Theoretical calculations and spectroscopic characterizations reveal that MBA reacts with FEC via nucleophilic substitutions, resulting in carbamate intermediates that are more susceptible to decomposition, thereby accelerating the nucleation of LiF during initial cycles.^[32] Such a process leads to the formation of a SEI with a LiF-rich inner layer with a lower impedance, which suppresses the formation of c-Li_{3.75}Si, maintaining the integrity of the electrode (Scheme 1). Consequently, the addition of 1 wt% of MBA to the baseline electrolyte (1.2 M LiPF₆ in ethylene carbonate (EC): diethyl carbonate (DEC) = 1:1 vol% with 10% FEC, denoted as EDF) leads to a substantial enhancement in cycling stability and rate performance. The resulting electrolyte (denoted as EDFM) also exhibits impressive cycling stability in pouch cells, underscoring their potential for practical applications. The proposed strategy, which regulates the formation of the SEI through intermediates, offers a novel approach for future electrolyte modifications.

Results and Discussion

Intermediate-Regulated SEI Formation

MBA, functioning as a nucleophilic agent, exhibits the inherent capability of its amine group to participate in nucleophilic substitution with the carbonyl carbon of FEC. [33,34] This chemical interaction leads to two distinct ring-opening scenarios, subsequently resulting in the formation of two intermediates, denoted as FM and FM2, respectively. In the electrolyte, the presence of LiPF₆ leads to the final chemical reaction products being FMLi and FM2Li, where hydroxyl hydrogens are replaced by Li (Figures 1a and S1). The reduction decomposition of the intermediates FMLi and FM2Li under

15213773, 2025, 33, Dowloaded from https://onlinelibrary.wiley.com/doi/10.1002/anie.202508832 by University Town Of Shenzhen, Wiley Online Library on [17/11/2025]. See the Terms and Conditions (https://onlinelibrary.wiley.com/doi/10.1002/anie.202508832 by University Town Of Shenzhen, Wiley Online Library on [17/11/2025]. See the Terms and Conditions (https://onlinelibrary.wiley.com/doi/10.1002/anie.202508832 by University Town Of Shenzhen, Wiley Online Library on [17/11/2025]. See the Terms and Conditions (https://onlinelibrary.wiley.com/doi/10.1002/anie.202508832 by University Town Of Shenzhen, Wiley Online Library on [17/11/2025]. See the Terms and Conditions (https://onlinelibrary.wiley.com/doi/10.1002/anie.202508832 by University Town Of Shenzhen, Wiley Online Library on [17/11/2025]. See the Terms and Conditions (https://onlinelibrary.wiley.com/doi/10.1002/anie.202508832 by University Town Of Shenzhen, Wiley Online Library on [17/11/2025]. See the Terms and Conditions (https://onlinelibrary.wiley.com/doi/10.1002/anie.202508832 by University Town Of Shenzhen, Wiley Online Library on [17/11/2025]. See the Terms and Conditions (https://onlinelibrary.wiley.com/doi/10.1002/anie.202508832 by University Town Of Shenzhen, Wiley Online Library on [17/11/2025]. See the Terms and Conditions (https://onlinelibrary.wiley.com/doi/10.1002/anie.20250882 by University Town Of Shenzhen, Wiley Online Library on [17/11/2025]. See the Terms and Conditions (https://onlinelibrary.wiley.com/doi/10.1002/anie.2025082 by University Town Of Shenzhen, Wiley Online Library on [17/11/2025]. See the Terms and Conditions (https://onlinelibrary.wiley.com/doi/10.1002/anie.2025082 by University Town Of Shenzhen, Wiley Online Library on [17/11/2025]. See the Terms and Conditions (https://onlinelibrary.wiley.com/doi/10.1002/anie.2025082 by University Town Of Shenzhen, Wiley Online Library on [17/11/2025]. See the Terms and Conditions (https://onlinelibrary.wiley.com/doi/10.1002/anie.2025082 by University Town Of Shenzhen, Wiley Online Library

-and-conditions) on Wiley Online Library for rules of use; OA articles are governed by the applicable Creative Commons

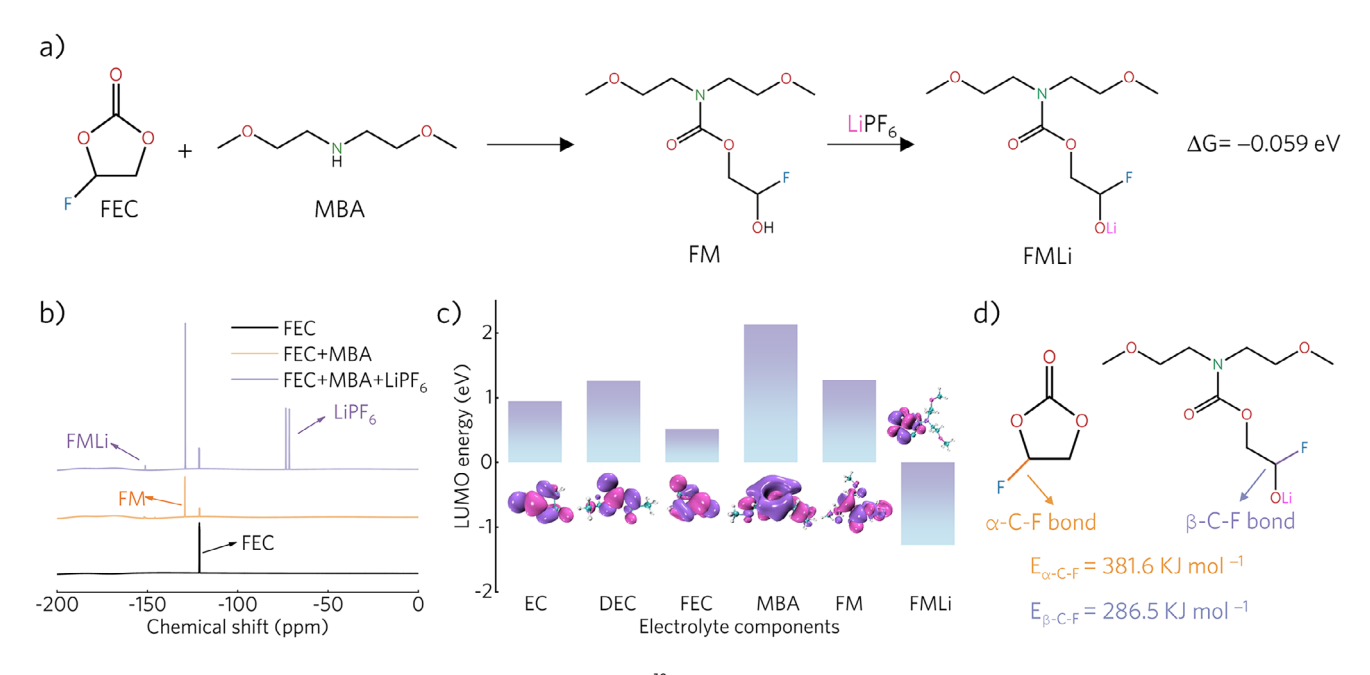


Figure 1. a) Possible degradation pathways of FEC induced by MBA. b) ¹⁹F NMR spectra of different electrolytes to verify reaction intermediates. c) LUMO energy levels of different electrolyte components. d) Bond energy analysis of FEC and the proposed intermediate.

electrochemical stimulation promotes LiF formation. Computation of the free energies associated with these pathways reveals that FMLi is the more spontaneously forming species, characterized by a Gibbs free energy of -0.059 eV, indicative of its propensity to proceed spontaneously.[35]

To confirm the occurrence of the above reactions, an electrolyte consisting of 1M LiPF₆ in a 1:1 vol% FEC: MBA mixture was prepared and characterized. ¹⁹F Nuclear Magnetic Resonance (NMR) spectroscopy identifies the possible characteristic peaks of the intermediates, FM at -129.0 ppm and FMLi at -151.2 ppm, confirming that the proposed chemical reaction between MBA and FEC indeed yields fluorine-containing intermediates (Figure 1b). In the analysis of LUMO energy levels among various electrolyte components, FMLi is found to have a significantly lower LUMO energy at -1.28 eV compared to other components, suggesting a preferential pathway for its reductive decomposition (Figure 1c).[36] Bond energy analysis further demonstrates that the β -C-F bond in the intermediate FMLi (286.5 KJ mol⁻¹) has significantly lower bond energy than those required for typical FEC reductive decomposition, specifically the α -C-F bond in FEC (381.6 KJ mol⁻¹) and $-nC_2H_3F$ - (460.8 KJ mol⁻¹ for n=2, a possible intermediate of typical FEC reduction). This result suggests a stronger tendency for the cleavage of the C-F bond, facilitating the formation of LiF (Figures 1d and S2).[37-39] To better reveal the reduction reaction process, the electrolyte composition variation during the initial cycle was monitored using in situ Fourier transform infrared (FTIR) spectroscopy (Figures 2a,b and S3).[40] It is essential to recognize that the baseline for FTIR signals is established at open-circuit voltage, and the measured reverse peaks indicate the consumption of certain electrolyte components near the electrode surface. The appearance of reverse peaks at 1772 cm⁻¹, 1802 cm⁻¹ (ν C=O)

and 728 cm⁻¹ (δ C–F)^[41,42] clearly indicates the consumption of FEC. Compared with the spectra obtained in EDF, where noticeable decomposition starts at around 1.2 V, the reduction in EDFM occurs at higher potentials (above 1.6 V). Therefore, the emergence of additive-induced intermediates is both thermodynamically and kinetically favorable for the rapid consumption of FEC, potentially resulting in a uniform SEI built upon a homogeneous foundational layer of LiF.

We have previously demonstrated that constructing a homogeneous passivation layer of LiF on the surface of SiO_x during the initial SEI formation stage is crucial for achieving a robust SEI.[43] To elucidate the formation of the SEI during the initial discharge cycle under the influence of additives, SiO_x||Li half-cells discharged to various discharge cutoff voltages were disassembled and characterized (Figures 2c and S4). The EDFM (EDF with 1 vol% MBA additive) group starts to decompose to form SEI at a relatively high voltage (~1.69 V), displaying a distinct reduction plateau, whereas such a plateau is barely observable in EDF, implying the promoting effect of MBA on SEI formation. Cyclic voltammetry (CV) results reveal distinct reduction peaks for FMLi and FEC at approximately 1.77 and 1.50 V, respectively (Figures S5 and S6), which correspond to the plateau observed in Figure 2c. Besides, the addition of MBA does not compromise the high-voltage stability of the electrolyte (Figure S7). SEM images (Figure S4) also demonstrate that under the same voltages, EDFM produces more decomposition products on SiO_x surface than the EDF group, confirming a higher degree of reduction reaction induced by MBA.

To determine the origin of the abovementioned reactions, X-ray photoelectron spectroscopy (XPS) was employed to measure the F atomic ratio (Figures 2d,e and S8) on the



15213773, 2025, 33, Downloaded from https://onlinelibrary.wiley.com/doi/10.1002/anie.202505832 by University Town Of Shenzhen, Wiley Online Library on [17/11/2025]. See the Terms

and Conditions (https://or

and-conditions) on Wiley Online Library for rules of use; OA articles are governed by the applicable Creative Commons

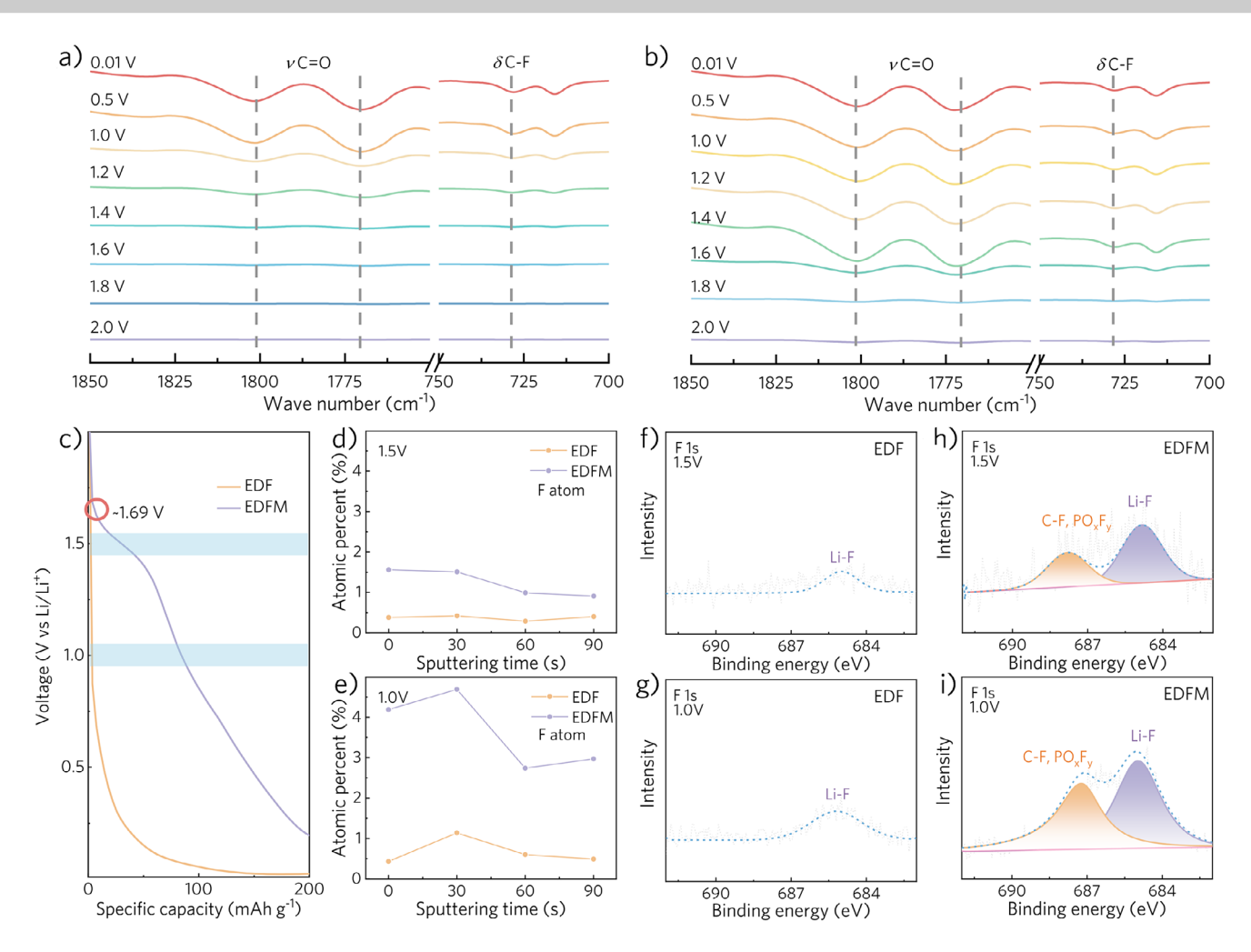


Figure 2. In situ FTIR monitoring of the electrode surface in a) EDF and b) EDFM during the first discharge cycle. c) Specific capacity-voltage curves during the first discharge cycle of SiO_x ||Li half-cells under 0.02 C. d), e) F contents on the surface of SiO_x anode at different discharge voltages (1.5 V and 1.0 V). XPS F Is spectra of SiO_x anodes in f), g) EDF and h), i) EDFM at various voltages.

electrode. At the initial reaction stage (1.5 V), EDFM shows a slightly higher F content than EDF (Figure 2d-h). As the voltage gradually decreases, the difference in F content between the two groups continues to widen, both on the surface and in the near-surface region, until it gradually stabilizes near the end of the reaction (0.01 V). Meanwhile, the carbon (C) content in EDF is comparable to that in EDFM at the early stages of the reaction, but becomes significantly higher than EDFM at the end of SEI formation (Figure S9 and Table S2). This suggests that the rapid decomposition of intermediates in EDFM can form a fluorine-rich inner SEI layer at an early stage to effectively passivate the anode surface and prevent side reactions. In contrast, the FEC in EDF follows a conventional decomposition route, [18,44] which fails to achieve early passivation at higher voltages, leading to extensive solvent decomposition at lower potentials and the formation of unstable organic SEI components.

To more precisely identify the types and origins of fluorinated products, F 1s spectra are analyzed. It is found that above 1.0 V, almost no C-F bond cleavage occurs in the EDF group, indicating that FEC remains largely undecomposed at this stage (Figures 2c,g and \$10).^[19] As the voltage further decreases, the C-F peak emerges at 0.5 V (Figure S11) and becomes stronger compared to Li-F peak at 0.01 V (Figure S12). This may be due to that previously formed SEI blocks the electron transfer pathways for FEC reduction, leading to its incomplete decomposition. In this view, without the formation of intermediates, the decomposition of FEC is not only unsatisfactory in terms of reaction rate, but also results in a lower yield of the target product (i.e., LiF and Table S2). In comparison, the C-F peak emerges at 1.5 V in the EDFM electrolyte (Figure 2h), indicating the formation of intermediate-derived composites in the SEI. This result well aligns with the in situ FTIR result where the decomposition of intermediate species occurs above 1.5 V. As the voltage continues to decrease, the relative intensity of the Li-F peak gradually increases (Figures 2h,i and S10-S12), indicating that SEI components derived from intermediates deposit on the electrode surface, allowing for continued electron transfer and the formation of the target LiF product.

15213773, 2025, 33, Downloaded from https://onlinelibrary.wiley.com/doi/10.1002/anie.202505832 by University Town Of Shenzhen, Wiley Online Library on [17/11/2025]. See the Terms

nditions) on Wiley Online Library for rules of use; OA articles are governed by the applicable Creative Commons

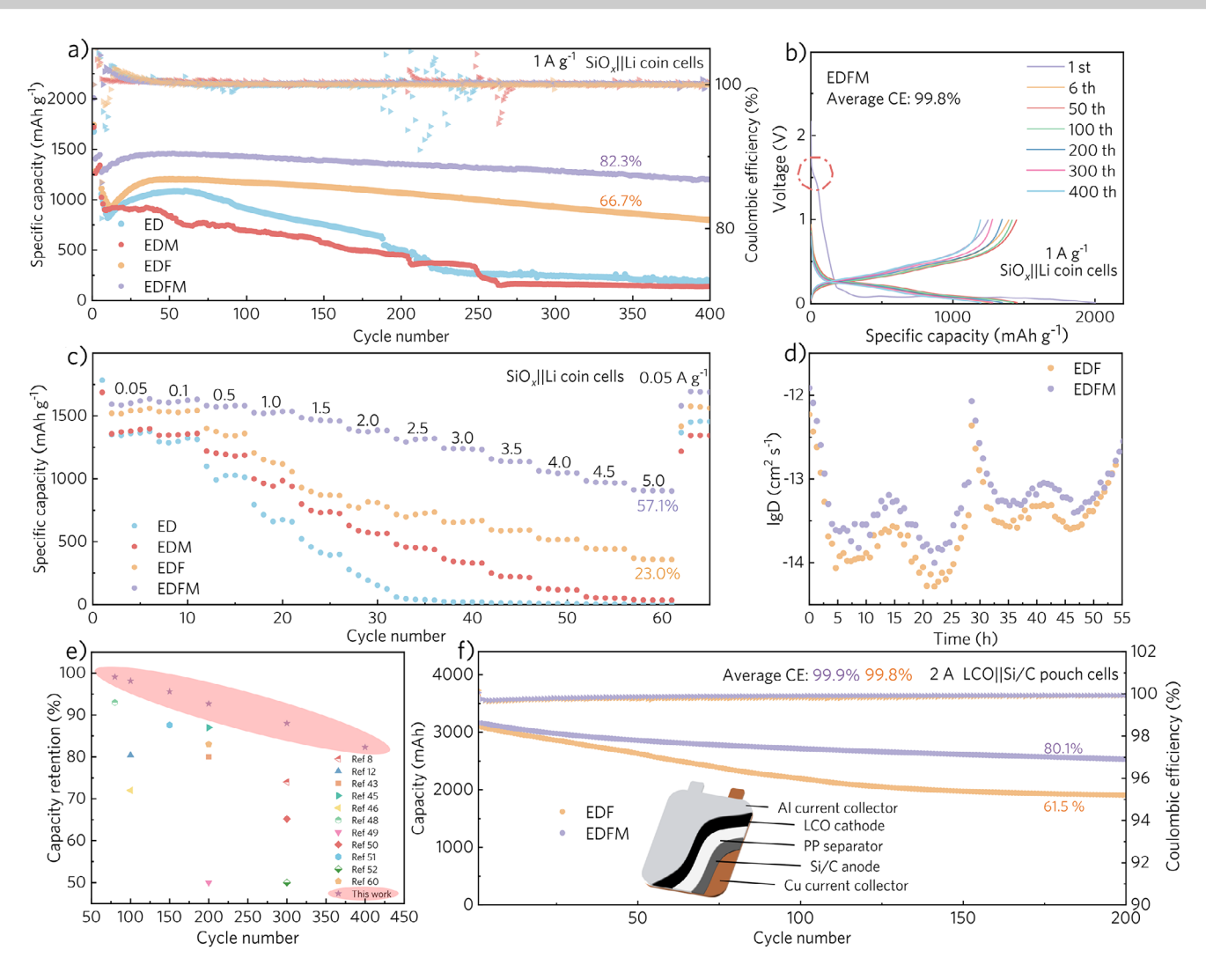


Figure 3. a) Cycling performance, b) galvanostatic charge/discharge profiles, and c) rate performance of $SiO_x||Li$ half-cells using different electrolytes. d) Time-diffusion coefficients of $SiO_x||Li$ half-cells with EDF and EDFM in GITT tests. e) A comparison of the cycling performance between this work and previous works on the interface modification of SiO_x anodes. f) Cycling performance of 3 Ah LCO||Si/C pouch cells cycled under the current of 2 A.

Enhanced Electrochemical Performance Enabled by LiF-Rich Inner SEI Layer

Next, SiO_x||Li half cells were fabricated to evaluate the electrochemical performance of four electrolytes. As baseline electrolytes, 1.2 m LiPF₆ in EC: DEC = 1:1 vol% (denoted as ED) and 1.2 M LiPF₆ in EC: DEC = 1:1 vol% with 1 vol% MBA (denoted as EDM) were prepared and tested for a more comprehensive comparison (Figure 3a). The first-cycle voltage profiles (Figure \$13) reveal a progressive decrease in initial coulombic efficiency (ICE) from 68.9% (ED) to 62.3% (EDFM) with sequential addition of FEC and MBA. This reduction likely reflects the additional electron consumption required for forming denser and more uniform electrodeelectrolyte interphases. In practical batteries, the reduced ICE can be compensated for by methods such as lithium supplementation. Furthermore, the cell with EDFM exhibits a distinctive voltage plateau around 1.6 V, corresponding to the intermediates decomposition discussed above (Figure \$14).

Due to the lack of a stable SEI, the capacity of the cells with ED and EDM decays rapidly, delivering capacity retentions of merely 189 and 141 mAh g⁻¹ after 400 cycles, respectively (Figure 3a). As for EDF, the peak discharge specific capacity reaches 1204 mAh g⁻¹ at the 50th cycle, resulting in a capacity retention rate of 66.7% after 400 cycles. The EDFM group, benefiting from the efficient SEI formation process, attains its maximum discharge specific capacity (1457 mAh g⁻¹) most rapidly within 46 cycles and maintains 82.3% of its peak capacity after 400 cycles, with an average coulombic efficiency (CE) of 99.8% (Figures 3b and S15). The cycling stability clearly demonstrates the importance of a stable LiF-rich inner layer SEI (Figure \$16). To further elucidate the electrochemical behavior, the DRT analysis of electrochemical impedance spectroscopy (EIS) data reveals distinct SEI evolution patterns between the two groups. The EDF control group exhibits progressively increasing $R_{\rm SEI}$ during cycling, suggesting SEI layer cracking and gradual thickening that hinders Li⁺ transport. In contrast, the EDFM group





demonstrates excellent $R_{\rm SEI}$ stability, which we attribute to its robust LiF-rich inner SEI structure (Figure S17 and Table S3). [45] Notably, in situ EIS measurements confirm that EDFM forms lower interfacial resistance during initial SEI formation, indicating rapid LiF nucleation that establishes highly ionic conductive pathways (Figure S18). [46] These ionic conductive networks effectively facilitate Li+ desolvation and enhance its charge transfer kinetics, ultimately leading to significantly reduced interfacial impedance.

In addition to cycle stability, the impact of different SEIs on rate performance was also evaluated (Figure 3c). The ED electrolyte shows poor rate performance, with virtually no discharge capacity left at a specific current of 5 A g⁻¹. EDM group exhibits a slightly better rate capability than the ED group, which may be attributed to Li₃N's role in facilitating ion transport kinetics.[47] After introducing FEC, EDF exhibits markedly improved rate performance by delivering a capacity of 368 mAh g⁻¹ (23.0%) even at 5 A g⁻¹. The EDFM electrolyte also achieves outstanding rate performance by exhibiting a discharge capacity of 923 mAh g^{-1} (57.1%) at 5 A g^{-1} , significantly outperforming both ED and EDF. It has been reported that nano-sized LiF components within the SEI not only stabilize the film but also establish a relatively superior ionic conductive network within the electrode, accelerating ion conduction and electron transport. [45,46] The galvanostatic intermittent titration technique (GITT) was utilized to assess the lithiumion diffusion coefficient (Figures 3d and S19). The energy barrier for Li⁺ penetrating through the SEI (designated as E_a) was also calculated using the Arrhenius equation, based on EIS data obtained at various temperatures (Figure S20 and Table S4). The EDFM, with an E_a of 30.9 kJ mol⁻¹, exhibits a markedly lower energy barrier than EDF, which has an E_a of 58.9 kJ mol⁻¹, thereby promoting more efficient lithium-ion transport. A comparison of the electrochemical performance of SiO_x with previous studies (Figure 3e and Table \$5) demonstrates that the interphase induced by EDFM provides superior cycling and rate performance.^[48–52] To evaluate the impact of MBA on full-cell performance, both LiNi_{0.8}Co_{0.1}Mn_{0.1}O₂||SiO_x coin cells and LiCoO₂||Si/C pouch cells were assembled (Figures 3f and S21-S25). The pouch cells employing the EDF electrolyte deliver an initial capacity with 61.5% retention after 200 cycles, demonstrating an average CE of 99.8%. In comparison, the EDFM system shows significantly improved performance, maintaining 80.1% capacity retention with a superior average CE of 99.9% over the same cycling period. Given that MBA can also significantly improve cycle performance in full cells, the proposed electrolyte modification strategy has very promising prospects for industrial application.

The Physical and Chemical Properties of SEI

To establish a correlation between the structure of the SEI and the cycling performance of the SiO_x anode, we conducted a series of characterizations on the SEI before and after cycling. First, scanning electron microscopy (SEM) and cryo-transmission electron microscopy (cryo-TEM) images

provide further insights into the morphology of the SEI (Figures 4a-d and S26-S27). SiO_x particles in both groups develop an SEI with a thickness of 30-40 nm. Employing the fast Fourier transform (FFT) mode, the EDFM group exhibits distinct micro-crystalline diffraction spots of LiF.[53] In contrast, the LiF diffraction spots are difficult to observe in the SEI formed by EDF (Figure 4a.c). The energy-dispersive spectroscopy (EDS) results also show that, compared to EDF, the SEI formed in EDFM contains a higher concentration of F (Figure \$28). This not only confirms the TEM results but also corroborates the XPS findings presented in Figures \$29 and \$30.^[54] After 200 cycles, the initially generated SEI in EDF, where LiF is randomly and sparsely distributed, exhibits inherent instability. Driven by the significant volume changes of the Si-based anode during cycling, this SEI undergoes dissolution and rupture, thereby exposing portions of the SiO_x surface (Figure 4b). In contrast, the uniformly formed LiF layer in the SEI derived from the EDFM shows superior morphological stability. Its enhanced mechanical strength and better adaptability to volume changes allow it to maintain the integrity of the SEI, providing a more robust protection for the anode (Figure 4d).

The componential stability of the SEI was further investigated by the O-K edge soft X-ray absorption spectroscopy (sXAS) in total electron yield (TEY) mode (Figure 4e,f). The O-K edge spectra of the pristine electrode clearly display the characteristic peaks of the silicon oxide (SiO₂) surface layer and the PAA binder. Both the EDF and EDFM groups exhibit prominent inorganic Li₂CO₃ and organic carbonates (LEMC, LEDC) on the surface of the electrodes after 5 cycles (Figure 4e).^[55] However, after 200 cycles, the SEI formed by EDF shows severe disintegration, with the typical SEI components' characteristic peaks (e.g., Li₂CO₃, LEMC, and LEDC) completely vanished, [55] suggesting exposure of the electrode surface (Figure 4f). In contrast, the surface O-K edge spectra of the SiO_x electrode cycled in EDFM remains stable after 200 cycles, showing evident characteristic peaks of the SEI components. Next, time-of-flight secondary-ion mass spectrometry (TOF-SIMS) was employed to assess the integrity and compositional distribution of the SEI after 3 and 200 cycles. LiF- fragments are used to illustrate the distribution of LiF components, while LiCO₃⁻, C₂HO⁻, and CH₂OF⁻ fragments are considered to correspond to the decomposition of carbonate solvents.^[56] Based on the depth profiles of ion fragments and the corresponding 3D visualization (Figures 4g and S31-S34), the EDF group forms a relatively uniform SEI film during the initial 3 activation cycles, although LiF components are predominantly distributed in the outer layer. After 200 cycles, the EDF electrode surface exhibits a heterogeneous distribution of LiF- fragments, characterized by irregular aggregation, accompanied by a diminished presence of LiCO₃⁻ and an uneven distribution of C₂HO⁻ and CH₂OF⁻, suggesting severe SEI disintegration during cycling. In contrast, the EDFM group consistently maintains a horizontally and vertically uniform distribution of LiFfragments, alongside evenly distributed LiCO₃-, C₂HO-, and CH₂OF⁻.

To evaluate the influence of LiF distribution on the mechanical properties of SEI layers, the atomic force

15213773, 2025, 33, Downloaded from https://onlinelibrary.wiley.com/doi/10.1002/anie.202505832 by University Town Of Shenzhen, Wiley Online Library on [17/11/2025]. See the Terms

ns) on Wiley Online Library for rules of use; OA articles are governed by the applicable Creative Commons

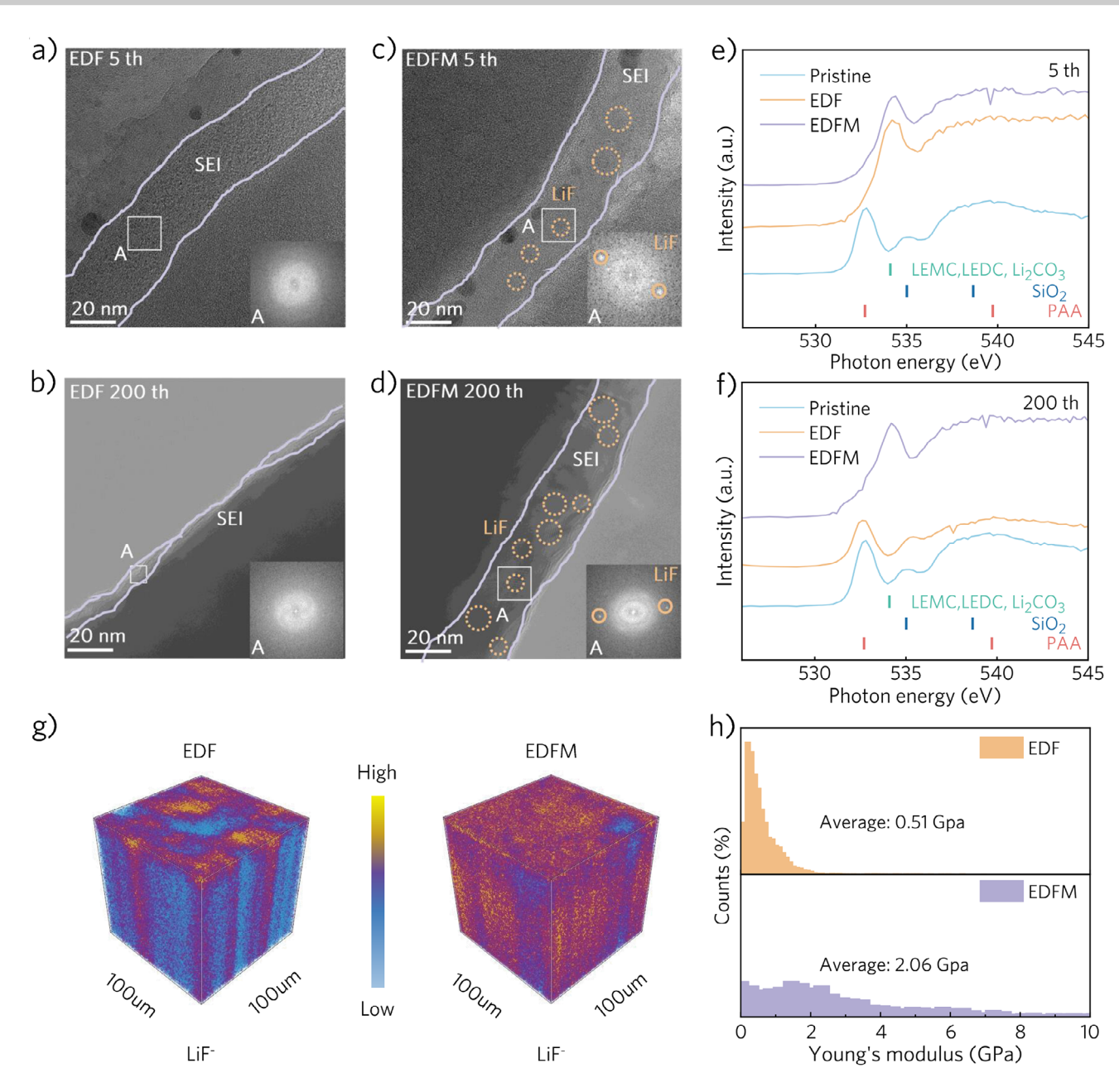


Figure 4. TEM images of SEI layers formed on SiO_x particles in a), b) EDF and c), d) EDFM after 5 and 200 cycles. e), f) O–K edge sXAS in the TEY mode for SiO_x anodes after 5 and 200 cycles. TOF-SIMS 3D visualization spectra of ion fragments on the surface of SiO_x anodes with EDF and EDFM after 200 cycles (g). DMT modulus distribution of SEI with EDF and EDFM measured via AFM after 5 cycles (h).

microscope (AFM) was employed to further measure the surface morphology and modulus. In contrast to the surface morphology of the SiO_x anode cycled in EDF (Figure S35), a more even surface is achieved in EDFM, which indicates the formation of a homogeneous SEI layer. Additionally, the Derjaguin–Müller–Toporov (DMT) modulus corresponding to the SiO_x anode cycled in EDFM is considerably greater than that in EDF, implying an enhancement in the mechanical strength of the SEI (Figure 4h). [12] The above results demonstrate that by facilitating the formation of LiF in the initial inner layer, the MBA additive enables the resulting SEI film to accommodate the volume changes of the SiO_x anode and maintain structural stability.

The Structural Integrity of SiO_x Particles Enabled by SEI

Under deep lithiation states (<50 mV versus Li/Li⁺), the formation of crystalline Li_{3.75}Si (c-Li_{3.75}Si) from the accumulation of amorphous Li_{3.75}Si (a-Li_{3.75}Si) induces significant lattice size variations of Si-based anodes, leading to material fracture and repeated degradation of the SEI.[57,58] In this sense, constructing an SEI with uniform mechanical properties and high lithium-ion conductivity plays a crucial role in preventing the formation of c-Li_{3.75}Si due to localized overlithiation.[59] The dQ/dV contour plots in the discharge process of the batteries are employed to depict the alloying process of SiO_x and the electrode evolution (Figure 5a). The

15213773, 2025, 33, Downloaded from https://onlinelibrary.wiley.com/doi/10.1002/anie.202505832 by University Town Of Shenzhen, Wiley Online Library on [17/11/2025]. See the Terms

litions) on Wiley Online Library for rules of use; OA articles are governed by the applicable Creative Commons Licens

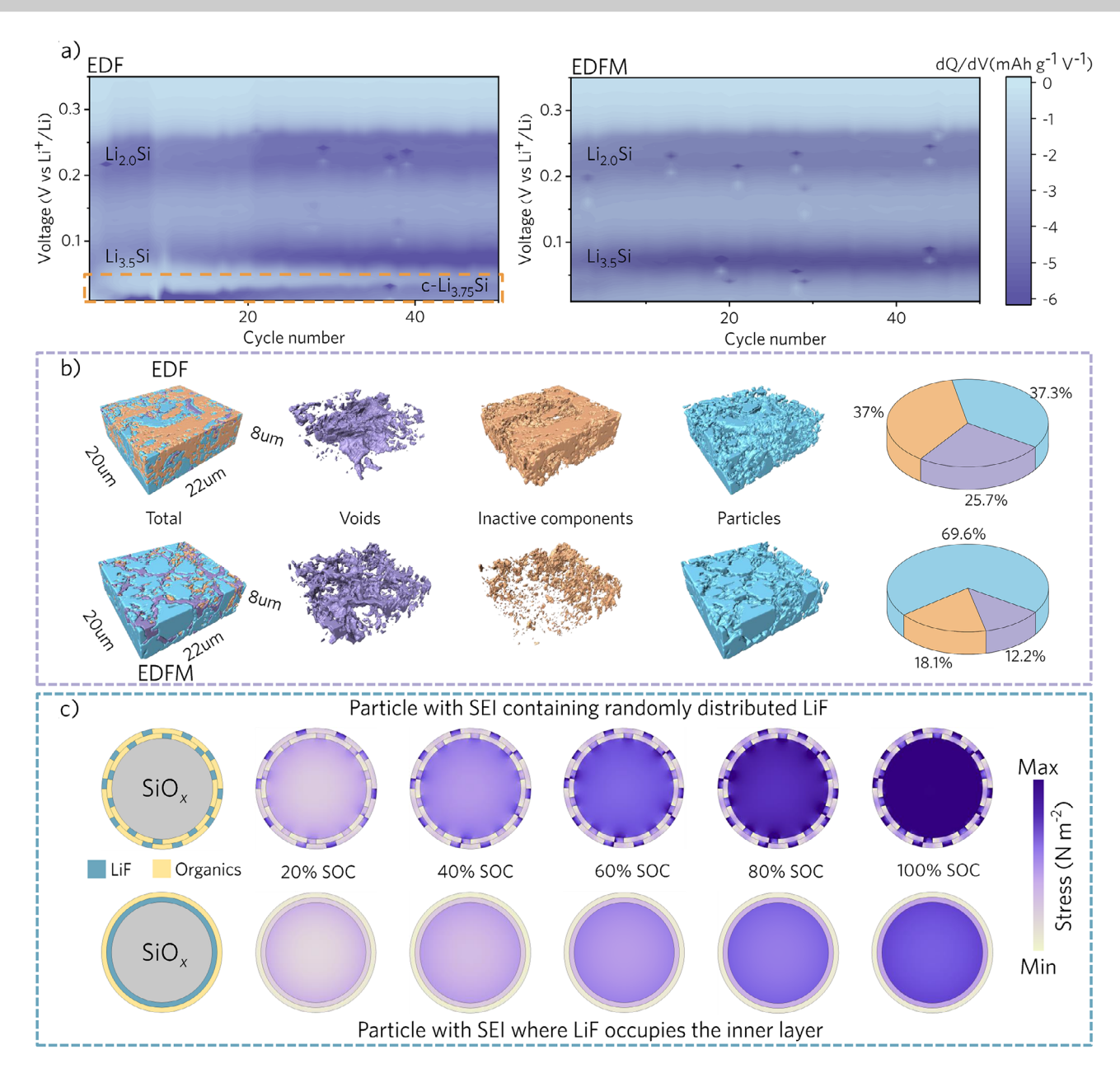


Figure 5. a) dQ/dV contour plots for the discharge process of $SiO_x||Li$ half-cells in EDF and EDFM. b) 3D visualization and the corresponding component pie charts of SiO_x anodes obtained by FIB-SEM after 200 cycles in EDF and EDFM. c) FEM simulations unveil the stress evolution of SiO_x particles under varying states of charge (SOC) influenced by different SEI configurations.

strong peaks emerging at 200–250 mV and 80 mV (indicated by the purple bands) are attributed to the formation of amorphous Li_{2.0}Si and Li_{3.5}Si. It is evident that after activation, the SiO_x||Li half-cells with EDFM remain nearly stable in the subsequent cycles, with the characteristic peak corresponding to the a-Li_{2.0}Si alloying process at 200–250 mV maintaining its peak width and intensity; the characteristic peak of the a-Li_{3.5}Si formation around 80 mV reaches its zenith within around 10 cycles and subsequently stabilize.^[60] In contrast, the incomplete activation of the EDF SiO_x||Li half-cell is revealed, with both peaks initially being low and only stabilizing after around 20 cycles. Notably, these two characteristic peaks in the EDF group are relatively broader than those in the EDFM group, which might have been a con-

sequence of the unstable electrode structure.^[60,61] Moreover, the EDF group exhibits the characteristic peak of c-Li_{3,75}Si under 50 mV (marked with a dashed border), indicating a more reversible volume change. To validate the inhibitory efficacy of the LiF-rich inner SEI in EDFM system against detrimental c-Li_{3,75}Si formation, we conducted systematic X-ray diffraction (XRD) characterization on SiO_x||Li half-cells at progressively decreasing discharge cutoff voltages (0.3, 0.1, 0.05, and 0.01 V) during the initial cycle (Figure S36). XRD analysis demonstrates that the EDF system shows detectable c-Li_{3,75}Si formation at 0.05 V with progressively intensified characteristic peaks at 0.01 V, while the EDFM system exhibits only marginal c-Li_{3,75}Si peak intensity at 0.01 V.^[4] The above analysis is also verified via in situ swelling ratio





tests (the cell configuration is shown in Figure S37). The swelling curves clearly indicate that the volume fluctuations in the cell using EDFM maintain stable within 3 cycles, indicating robust structural stability (Figure S38); whereas the cell using EDF shows an increasing swelling ratio as the cycling proceeds (reaching 181% within 3 cycles), such irreversible volume change can be attributed to the thickening of the SEI layer. [8,21]

Next, by employing a combination of focused ion beam and scanning electron microscopy (FIB-SEM), 3D image reconstruction of SiO_x electrodes was carried out to visualize the effect of SEI on the structural integrity of electrodes (Figure 5b). Based on the differences in contrast among various components, the 3D structure of SiO_x anodes can be segmented into voids, inactive components (e.g., SEI, binder, and conductive carbon), and SiO_x particles.^[21] Compared with the EDFM group, the EDF group shows significantly higher ratios of voids and inactive components, which undermines the integrity of conductive networks. The structural instability originates from two aspects: on one hand, due to the continuous side reactions at the interface, the SEI undergoes unrestricted thickening, leading to an increase in inactive components and the formation of pores; on the other hand, uneven stress on the particle surfaces causes nonuniform expansion and contraction of the electrode, further triggering structural damage. Conversely, EDFM helps the SiOx anode form a SEI film rich in LiF with uniform morphology and composition as well as high conductivity, effectively reducing the damage to the electrode structure caused by volume changes during cycling. To investigate the stress evolution in SiO_x anodes with different electrolytes, we developed finite element models (FEM) of SiO_x particles covered by SEI layers: one with LiF occupying the inner layer and the other with randomly dispersed LiF particles, using the COMSOL Multiphysics simulation platform. [62] The stress distribution resulting from lithium concentration gradients during electrochemical cycling was quantified through a coupled electrochemical-mechanical approach (Figure 5c). The SiO_x particle coated with an SEI layer containing randomly dispersed LiF demonstrates substantial stress accumulation during lithiation. Conversely, SiO_x particles with a hierarchically structured SEI layer exhibit significantly lower stress accumulation, suggesting improved structural stability, which can be attributed to the high Young's modulus and low adhesion properties of the LiF-rich inner SEI layer. [63,64] These results demonstrate that the SEI film, with its MBA additive-induced LiF-rich inner layer and mechanical robustness, significantly enhances the electrochemical reversibility of SiO_x , suppresses the formation of the structurally unstable c-Li_{3.75}Si phase, mitigates irreversible volume changes during cycling, and minimizes stress accumulation, thereby preserving the structural integrity of the SiO_x particles.

Conclusion

In this study, to promote the conversion of commercial electrolyte additive FEC into the target SEI product LiF, MBA, a proton acceptor additive, is introduced into the

electrolyte. MBA attacks the carbonyl group of FEC to form an intermediate (FMLi), which is both thermodynamically and kinetically favorable for electrochemical reduction. Consequently, an SEI with a desirable structure, featuring a LiF-rich inner layer, is constructed on SiO_x anodes. The stable SEI, with high mechanical durability and fast lithiumion transport capability, mitigates irreversible volume changes and SEI degradation, ensuring stable cycling and excellent rate performance of the SiO_x anodes. The SiO_x||Li half-cells retain 82.3% of their capacity after 400 cycles and obtain a capacity retention rate of 57.1% at 5 A g⁻¹. The stable cycling of pouch full cells further highlights the practical value of this electrolyte modification strategy, which modulates SEI formation via intermediates. This approach not only enhances the efficiency of commonly used additives but also opens up new avenues for optimizing electrolyte formulations to improve the performance and longevity of next-generation lithium-ion batteries.

Acknowledgements

This work was supported by the Major Science and Technology Infrastructure Project of Material Genome Big-science Facilities Platform supported by the Municipal Development and Reform Commission of Shenzhen, the Basic and Applied Basic Research Foundation of Guangdong Province (No. 2021B1515130002), the International Joint Research Center for Electric Vehicle Power Battery and Materials (No. 2015B01015), the Guangdong Key Laboratory of Design and Calculation of New Energy Materials (No. 2017B030301013), the Shenzhen Key Laboratory of New Energy Resources Genome Preparation and Testing (No. ZDSYS201707281026184), and the Shenzhen Science and Technology Planning Project (No. JSGG20220831095604008).

Conflict of Interests

The authors declare no conflict of interest.

Data Availability Statement

The data that support the findings of this study are available from the corresponding author upon reasonable request.

Keywords: Cycling stability • Electrolytes • Intermediates • Si-based anodes • Solid-electrolyte interphase

- [1] S. Chae, M. Ko, K. Kim, K. Ahn, J. Cho, Joule 2017, 1, 47-60.
- [2] P. Ruvinskiy, I. V. Barsukov, O. Mashtalir, C. M. Reid, J. J. Wu, Y. Gogotsi, Ecs. J. Solid State Sc. 2013, 2, M3028–M3033.
- [3] J. Xie, Y. C. Lu, Nat. Commun. 2020, 11, 2499.
- [4] T. Liu, T. T. Dong, M. Y. Wang, X. F. Du, Y. L. Sun, G. J. Xu, H. R. Zhang, S. M. Dong, G. L. Cui, *Nat. Sustain.* 2024, 7, 1057– 1066.
- [5] Y. Jin, S. Li, A. Kushima, X. Q. Zheng, Y. M. Sun, J. Xie, J. Sun, W. J. Xue, G. M. Zhou, J. Wu, F. F. Shi, R. F. Zhang, Z. Zhu, K. P. So, Y. Cui, J. Li, *Energ. Environ. Sci.* 2017, 10, 580–592.





- [6] G. Y. Qian, X. H. Chen, H. Lin, L. Y. Yang, Cell. Rep. Phys. Sci. 2024, 5, 102153.
- [7] J. R. Sun, G. D. Chen, B. Wang, J. D. Li, G. J. Xu, T. Y. Wu, Y. F. Tang, S. M. Dong, J. Y. Huang, G. L. Cui, *Angew. Chem. Int. Ed.* 2024, 63, e202406198.
- [8] G. Y. Qian, Y. W. Li, H. B. Chen, L. Xie, T. C. Liu, N. Yang, Y. L. Song, C. Lin, J. F. Cheng, N. Nakashima, M. Zhang, Z. K. Li, W. G. Zhao, X. J. Yang, H. Lin, X. Lu, L. Y. Yang, H. Li, K. Amine, L. Q. Chen, F. Pan, *Nat. Commun.* 2023, 14, 6048.
- [9] X. C. Zhuang, S. H. Zhang, Z. L. Cui, B. Xie, T. Y. Gong, X. H. Zhang, J. D. Li, R. X. Wu, S. T. Wang, L. X. Qiao, T. Liu, S. M. Dong, G. J. Xu, L. Huang, G. L. Cui, *Angew. Chem. Int. Ed.* 2024, 63, e202315710.
- [10] J. R. Sun, L. Huang, G. J. Xu, S. M. Dong, C. S. Wang, G. L. Cui, Mater. Today 2022, 58, 110–118.
- [11] C. K. Chan, H. L. Peng, G. Liu, K. McIlwrath, X. F. Zhang, R. A. Huggins, Y. Cui, Nat. Nanotechnol. 2008, 3, 31–35.
- [12] S. M. Chen, G. R. Zheng, X. M. Yao, J. L. Xiao, W. G. Zhao, K. Li, J. J. Fang, Z. N. Jiang, Y. X. Huang, Y. C. Ji, K. Yang, Z. W. Yin, M. Zhang, F. Pan, L. Y. Yang, ACS Nano 2024, 18, 6600–6611.
- [13] S. M. Chen, Z. B. Song, L. Wang, H. Chen, S. Q. Zhang, F. Pan, L. Y. Yang, Acc. Chem. Res. 2022, 55, 2088–2102.
- [14] Y. H. Tan, Z. Liu, J. H. Zheng, Z. J. Ju, X. Y. He, W. Hao, Y. C. Wu, W. S. Xu, H. J. Zhang, G. Q. Li, L. S. Zhou, F. Zhou, X. Y. Tao, H. B. Yao, Z. Liang, Adv. Mater. 2024, 36, 2404815.
- [15] D. J. Yoo, S. Yang, K. J. Kim, J. W. Choi, Angew. Chem. Int. Ed. 2020, 59, 14869–14876.
- [16] S. Y. Li, J. N. Li, P. Wang, H. Ding, J. F. Zhou, C. Y. Li, X. L. Cui, Adv. Funct. Mater. 2024, 34, 2307180.
- [17] S. Y. Li, Y. L. Zhang, S. M. Wu, Y. Quan, M. L. Wu, P. Wang, D. N. Zhao, X. L. Cui, *Chem. Eng. J.* **2024**, 485, 150095.
- [18] E. Markevich, G. Salitra, D. Aurbach, ACS Energy Lett. 2017, 2, 1337–1345
- [19] Y. T. Dong, Y. M. Chen, X. Y. Yue, Z. Liang, Energ. Environ. Sci. 2024, 17, 2500–2511.
- [20] H. Zhang, Z. Song, K. Yang, Y. Zhou, Y. Ji, L. Wang, Y. Huang, S. Xu, J. Fang, W. Zhao, G. Qian, S. Wu, J. V. Anguita, G. F. Trindade, S. Xue, H. Wang, I. S. Gilmore, Y. Zhao, F. Pan, Adv. Energy Mater. 2025, 2406104.
- [21] C. Zhu, S. M. Chen, K. Li, Z. W. Yin, Y. G. Xiao, H. Lin, F. Pan, L. Y. Yang, Sci. Bull. 2023, 68, 408–416.
- [22] Q. Li, X. S. Liu, X. Han, Y. X. Xiang, G. M. Zhong, J. Wang, B. Z. Zheng, J. G. Zhou, Y. Yang, ACS Appl. Mater. Interfaces 2019, 11, 14066–14075.
- [23] C. Xu, F. Lindgren, B. Philippe, M. Gorgoi, F. Björefors, K. Edström, T. Gustafsson, *Chem. Mater.* 2015, 27, 2591–2599.
- [24] I. A. Profatilova, C. Stock, A. Schmitz, S. Passerini, M. Winter, J. Power Sources 2013, 222, 140–149.
- [25] Y. C. Li, Z. Cao, Y. Wang, L. Z. Lv, J. Y. Sun, W. X. Xiong, Q. T. Qu, H. H. Zheng, ACS Energy Lett. 2023, 8, 4193–4203.
- [26] Y. T. Jin, N. J. H. Kneusels, L. E. Marbella, E. Castillo-Martínez, P. C. M. M. Magusin, R. S. Weatherup, E. Jónsson, T. Liu, S. Paul, C. P. Grey, J. Am. Chem. Soc. 2018, 140, 9854–9867.
- [27] G. M. Veith, M. Doucet, J. K. Baldwin, R. L. Sacci, T. M. Fears, Y. Q. Wang, J. F. Browning, J. Phys. Chem. C 2015, 119, 20339– 20349.
- [28] J. D. McBrayer, M. T. F. Rodrigues, M. C. Schulze, D. P. Abraham, C. A. Apblett, I. Bloom, G. M. Carroll, A. M. Colclasure, C. Fang, K. L. Harrison, G. Liu, S. D. Minteer, N. R. Neale, G. M. Veith, C. S. Johnson, J. T. Vaughey, A. K. Burrell, B. Cunningham, *Nat. Energy.* 2021, 6, 866–872.
- [29] J. Wang, Z. Yang, B. G. Mao, Y. X. Wang, Y. Jiang, M. H. Cao, ACS Energy Lett. 2022, 7, 2781–2791.
- [30] P. Mishra, N. S. Kiran, L. F. R. Ferreira, K. K. Yadav, S. I. Mulla, Chemosphere 2023, 326, 138391.

- [31] Y. J. Song, R. Y. Li, G. Y. Chen, B. B. Yan, L. Zhong, Y. X. Wang, Y. H. Li, J. L. Li, Y. X. Zhang, *Int. J. Env. Res. Pub. He.* 2021, 18, 8859.
- [32] K. Stagel, L. Ielo, K. Bica-Schröder, ACS Omega 2023, 8, 48444– 48450
- [33] K. Verma, A. Sharma, J. Singh, R. Badru, Sustain. Chem. Pharm. 2021, 20, 100377.
- [34] B. Ochiai, Y. Satoh, T. Endo, J. Polym. Sci. Pol. Chem. 2009, 47, 4629–4635.
- [35] Y. H. Gao, G. Wu, W. Q. Fang, Z. S. Qin, T. Zhang, J. X. Yan, Y. P. Zhong, N. Zhang, G. Chen, *Angew. Chem. Int. Ed.* **2024**, *63*, e202403668.
- [36] P. Peljo, H. H. Girault, Energ. Environ. Sci. 2018, 11, 2306–2309.
- [37] N. von Aspern, G. V. Roeschenthaler, M. Winter, I. Cekic-Laskovic, Angew. Chem. Int. Ed. 2019, 58, 15978–16000.
- [38] Y. T. Jin, N. J. H. Kneusels, P. C. M. M. Magusin, G. Kim, E. Castillo-Martínez, L. E. Marbella, R. N. Kerber, D. J. Howe, S. Paul, T. Liu, C. P. Grey, J. Am. Chem. Soc. 2017, 139, 14992–15004.
- [39] D. Aurbach, E. Markevich, G. Salitra, J. Am. Chem. Soc. 2021, 143, 21161–21176.
- [40] Y. Huang, Y. Ji, G. Zheng, H. Cao, H. Xue, X. Yao, L. Wang, S. Chen, Z. Yin, F. Pan, L. Yang, CCS Chem. 2025, 7, 429–439.
- [41] Y. B. Yohannes, S. D. Lin, N. L. Wu, B. J. Hwang, J. Electrochem. Soc. 2019, 166, A2741–A2748.
- [42] B. N. Olana, L. H. Adem, S. D. Lin, B. J. Hwang, Y. C. Hsieh, G. Brunklaus, M. Winter, ACS Appl. Energ. Mater. 2023, 6, 4800– 4809
- [43] S. M. Chen, Z. K. Deng, J. X. Li, W. G. Zhao, B. W. Nan, Y. Zuo, J. J. Fang, Y. X. Huang, Z. W. Yin, F. Pan, L. Y. Yang, *Angew. Chem. Int. Ed.* 2025, 64, e202413927.
- [44] P. G. Kitz, M. J. Lacey, P. Novák, E. J. Berg, J. Power Sources 2020, 477, 228567.
- [45] R. X. Wu, X. F. Du, T. Liu, X. C. Zhuang, P. Guan, B. Q. Zhang, S. H. Zhang, C. H. Gao, G. J. Xu, X. H. Zhou, G. L. Cui, Adv. Energy Mater. 2024, 14, 2302899.
- [46] R. L. Li, B. H. Cui, Q. J. Zhou, X. Mu, Y. Z. Gao, G. P. Yin, C. K. Fu, P. J. Zuo, J Energy. Chem. 2023, 86, 32–40.
- [47] Y. B. He, P. C. Zou, S. M. Bak, C. Y. Wang, R. Zhang, L. B. Yao, Y. H. Du, E. Y. Hu, R. Q. Lin, H. L. Xin, ACS Energy Lett. 2022, 7, 2866–2875.
- [48] S. J. Ko, X. Han, T. Shimada, N. Takenaka, Y. Yamada, A. Yamada, Nat. Sustain. 2023, 6, 1705–1714.
- [49] Y. F. Tian, S. J. Tan, Z. Y. Lu, D. X. Xu, H. X. Chen, C. H. Zhang, X. S. Zhang, G. Li, Y. M. Zhao, W. P. Chen, Q. Xu, R. Wen, J. Zhang, Y. G. Guo, Angew. Chem. Int. Ed. 2023, 62, e202305988.
- [50] Z. J. Xu, R. Huang, P. F. Huang, C. W. He, S. W. Liu, H. N. Zheng, W. L. Song, L. Shi, W. W. Gao, D. Li, H. Huang, H. J. Ying, W. Q. Han, Chem. Eng. J. 2024, 500, 157028.
- [51] L. B. Huang, L. Zhao, Z. F. Ma, X. Zhang, X. S. Zhang, Z. Y. Lu, G. Li, X. X. Luo, R. Wen, S. Xin, Q. H. Meng, Y. G. Guo, *Angew. Chem. Int. Ed.* 2024, 63, e202413600.
- [52] C. L. Li, Y. Zhu, Y. Quan, F. F. Zong, J. Wang, D. N. Zhao, N. S. Zhang, P. Wang, X. L. Cui, S. Y. Li, *J Energy. Chem.* **2024**, 98, 680–691.
- [53] G. M. Hobold, C. Z. Wang, K. Steinberg, Y. Z. Li, B. M. Gallant, Nat. Energy. 2024, 9, 580–591.
- [54] Z. H. Wu, C. Y. Wang, Z. Y. Hui, H. D. Liu, S. Wang, S. C. Yu, X. Xing, J. Holoubek, Q. S. Miao, H. L. Xin, P. Liu, *Nat. Energy.* 2023, 8, 226–227.
- [55] F. Wu, Y. Dong, Y. F. Su, C. X. Wei, T. R. Chen, W. A. Yan, S. Y. Ma, L. Ma, B. Wang, L. Chen, Q. Huang, D. Y. Cao, Y. Lu, M. Wang, L. Wang, G. Q. Tan, J. H. Wang, N. Li, Small 2023, 19, 2301301.
- [56] B. D. Zhang, X. H. Wu, H. Y. Luo, H. Yan, Y. L. Chen, S. Y. Zhou, J. H. Yin, K. Zhang, H. G. Liao, Q. S. Wang, Y. G. Zou, Y. Qiao, S. G. Sun, J. Am. Chem. Soc. 2024, 146, 4557–4569.





1521 3773, 2025, 33, Downloaded from https://onlinelibrary.wiley.com/doi/10.1002/anie.202505832 by University Town Of Shenzhen, Wiley Online Library on [17/11/2025]. See the Terms

- [57] K. Ogata, E. Salager, C. J. Kerr, A. E. Fraser, C. Ducati, A. J. Morris, S. Hofmann, C. P. Grey, Nat. Commun. 2014, 5, 3217.
- [58] M. Gu, Z. G. Wang, J. G. Connell, D. E. Perea, L. J. Lauhon, F. Gao, C. M. Wang, ACS Nano 2013, 7, 6303–6309.
- [59] H. Z. Xie, S. Y. Sayed, W. P. Kalisvaart, S. J. Schaper, P. Müller-Buschbaum, E. J. Luber, B. C. Olsen, M. Haese, J. M. Buriak, ACS Appl. Energ. Mater. 2020, 3, 1609–1616.
- [60] Y. F. Tian, G. Li, D. X. Xu, Z. Y. Lu, M. Y. Yan, J. Wan, J. Y. Li, Q. Xu, S. Xin, R. Wen, Y. G. Guo, Adv. Mater. 2022, 34, 2200672.
- [61] H. Y. Ren, J. X. Hu, H. C. Ji, Y. X. Huang, W. G. Zhao, W. Y. Huang, X. H. Wang, H. C. Yi, Y. L. Song, J. J. Liu, T. C. Liu, M. Liu, Q. H. Zhao, F. Pan, Adv. Mater. 2024, 36, 2408875.
- [62] S. F. Lou, Q. W. Liu, F. Zhang, Q. S. Liu, Z. J. Yu, T. S. Mu, Y. Zhao, J. Borovilas, Y. J. Chen, M. Y. Ge, X. H. Xiao, W. K. Lee,

- G. P. Yin, Y. Yang, X. L. Sun, J. J. Wang, Nat. Commun. 2020, 11, 5700
- [63] J. Chen, X. L. Fan, Q. Li, H. B. Yang, M. R. Khoshi, Y. B. Xu, S. Hwang, L. Chen, X. Ji, C. Y. Yang, H. X. He, C. M. Wang, E. Garfunkel, D. Su, O. Borodin, C. S. Wang, *Nat. Energy.* 2020, 5, 386–397.
- [64] T. Y. Yu, T. Zhao, N. X. Zhang, T. Y. Xue, Y. Chen, Y. S. Ye, F. Wu, R. J. Chen, *Nano Lett.* 2023, 23, 276–282.

Manuscript received: March 13, 2025 Revised manuscript received: June 12, 2025 Accepted manuscript online: June 12, 2025 Version of record online: June 23, 2025

are governed by the applicable Creative Commons